Rev. Adv. Mater. Sci. 57 (2018) 183-192

# EFFECT OF CARBON SOURCES AND SYNTHESIS CONDITIONS ON THE $LiFePO_4$/C CATHODE PROPERTIES

**R.R. Kapaev[1,2], S.A. Novikova[1], A.A. Chekannikov[2], D.Yu. Gryzlov[3], T.L. Kulova[3], A.M. Skundin[3] and A.B. Yaroslavtsev[1]**

[1]Kurnakov Institute of General and Inorganic chemistry of Russian Academy of Sciences, 31 Leninsky pr., 119991 Moscow, Russia
[2]Skolkovo Intitute of Science and Technology, 3 Nobel st., 143026 Moscow, Russia
[3]Frumkin Institute of Physical chemistry and Electrochemistry of Russian Academy of Sciences, 31-4 Leninsky pr., 119071 Moscow, Russia

*Received: February 26, 2018*

**Abstract.** The sol-gel synthesis and precipitation from dimethyl sulfoxide (DMSO)-water mixture were used to obtain $LiFePO_4$. Sucrose (sucr), citric acid (CA), phthalic acid (phth), polyvinyl alcohol (PVA), polyvinylpyrrolidone (PVP), polyvinylidene fluoride (PVDF), polyethylene glycol (PEG), polyacrylic acid (PAA) were investigated as carbon precursors. Increasing of the annealing temperature from 600 °C to 800 °C leads to a certain perfection of graphite structure with simultaneous particle size growth. Higher capacities were observed for the materials synthesized at 600 °C. The best results for the sol-gel synthesis were obtained when PVDF was used as a source of carbon coating due to the partial fluorination of $LiFePO_4$ (discharge capacity of $LiFePO_4$/C-PVDF was ~160 and 70 mAh $g^{-1}$ at 20 mA $g^{-1}$ and 800 mA $g^{-1}$ currents, respectively). For nanocrystalline $LiFePO_4$ obtained by precipitation from DMSO-water mixture the best results were obtained when PEG was used as carbon source (discharge capacity $LiFePO_4$/C-PEG was 158 and 77 mAh $g^{-1}$ at 20 mA $g^{-1}$ and 800 mA $g^{-1}$, respectively).

## 1. INTRODUCTION

Lithium iron phosphate with olivine structure $LiFePO_4$ (LFP) has drawn attention as a cathode material due to low cost, safety, stability and comparatively high theoretical capacity (170 mAh·$g^{-1}$) [1]. The prime limitation to using $LiFePO_4$ as a cathode material is its low electrical conductivity. Electron conduction of the material at room temperature is on the order of $10^{-9}$ S·$cm^{-1}$, and lithium ion diffusion coefficient is ~$10^{-14}$-$10^{-16}$ $cm^2$·$s^{-1}$ [2,3]. Low electrical conductivity results in a dramatic drop of charge and discharge capacities with increasing current density and limits the applicability of this material in devices that require a high on-peak power [4].

Among the modification methods of LFP-based cathode materials, which make it possible to overcome the limitations associated with low electrical conductivity of these materials, of particular interest are the preparation of nanomaterials [5-9], partial substitution of iron ions for other metal ions [9-15], formation of composite materials [6,16-28]. As a result of particle size reduction, surface area of the material increases, enhancing the contact with the electrolyte, while the diffusion length to the intergrain space, where charge transfer generally occurs markedly faster than in crystals, shortens [8,29].

Partial substitution of structure-forming ions in LFP (doping) is performed to improve the bulk conductivity of the material. This approach is based on

Corresponding author: A.B. Yaroslavtsev, e-mail: yaroslav@igic.ras.ru

formation of additional point defects in the bulk of solids, the migration of which determines the ion transfer [30]. In some cases, this approach makes it possible to achieve higher charge and discharge current densities, while maintaining relatively high capacity [10,11,13-15,31-33] or to increase the working potential of a cathode material via the electrochemical activity of dopant ions. For example, when the material is doped with manganese, an additional plateau appears on the charge/discharge curve at the potential of 4.1 V [13,15].

Formation of composites with conductive additives increases electron transfer at the grain boundary. Polymers, such as polyaniline (PANI), polypyrrole (PPy) or poly(3,4-ethylenedioxythiophene) (PEDOT) [16,35-38], as well as various forms of carbon (amorphous carbon, graphite, graphene, carbon nanotubes) [39-43] are used as conductive additives. The main advantage of carbon additives is their availability and low cost. Among the possible carbon sources are carbohydrates [44-46], carboxylic acids [47,48], polyvinyl alcohol [49], hydrocarbons [50], polyvinylidene fluoride [19] or polyaniline [51,52]. Carbon coating of active material particles is performed in most cases by adding a carbon source to the cathode material, followed by thermal decomposition in an inert atmosphere [44-46]. Along with increasing of electrical conductivity, the formed carbon coating prevents sintering of LFP particles during the annealing process and promotes the formation of a more finely dispersed material. The morphology of a LFP/C product can be dramatically influenced by the choice of synthesis method and final annealing temperature, which, in turn, influences both discharge capacities and their retention at higher charge/discharge rates, as well as the stability of an LFP/C-based cathode material [53].

The aim of this study was to compare different synthesis methods of LFP/C composites and to define the influence of synthesis conditions and carbon coating source on the electrochemical performance of $LiFePO_4$/C as a cathode in lithium-ion battery operation mode. Since graphite ($sp^2$-hybridization) is generally characterized by higher conductivity, carbon coatings with high graphite content are more preferable [54-56]. According to the reported data, pyrolysis of organic compounds having aromatic fragments yields carbon with high graphite content [54-57]. Various organic compounds with low or high molecular weights, which have different substituents and aliphatic or aromatic moieties, were tested as carbon sources.

## 2. EXPERIMENTAL

Synthesis of LFP/C materials was carried out: {I} using sol-gel method following a previously reported procedure [6], and {II} by precipitation from DMSO-water mixture as described elsewhere [58]. For the procedure {I} $Fe(NO_3)_3 \cdot 9H_2O$ (Sigma-Aldrich, >98%), $LiNO_3$ (Sigma-Aldrich, >98%), $NH_4H_2PO_4$ (Sigma-Aldrich, >98%) in stoichiometric ratio were used as precursors. The reagents were dissolved in deionized water, the resulting solution was evaporated and the residue was then annealed at 300 °C, producing LFP precursor, and afterwards at 600-800 °C in the argon atmosphere.

For the procedure {II} LiOH (Sigma-Aldrich, 98%), $FeSO_4 \cdot 7H_2O$ (Sigma-Aldrich, 99.5+%), $H_3PO_4$ (Chimmed, 85%) and ascorbic acid (Fischer Scientific, 99+%) in a molar ratio 3:1:1:0.05 were added to the DMSO-water mixture (volumetric ratio DMSO: $H_2O$ = 1:1) in the $N_2$ atmosphere. The mixture was heated to the boiling point (108 °C) and kept at constant stirring for 3 hours. After cooling the precipitate was collected by centrifugation, washed with water and dried in a vacuum drying chamber at 40 °C.

Several organic compounds, which contain heteroatoms (O,F,N) to ensure adsorption on the surface of inorganic compounds, were used as a carbon coating sources. Among them are both low-molecular-weight, such as sucrose (Sigma Aldrich, 99+%), citric acid (Sigma Aldrich, 99%), phthalic acid (Sigma Aldrich, 99.5+%), and high-molecular-weight, such as polyvinyl alcohol (Mark 16/1, $M_W$ ~78000), polyvinylpyrrolidone (PVP) (Sigma Aldrich, $M_W$ ~40000), polyvinylidene fluoride (Sigma Aldrich, $M_W$ ~$1.07 \cdot 10^5$), polyethylene glycol (ABCR, $M_W$~4000), polyacrylic acid (Sigma Aldrich, $M_W$~450000). The carbon source was added to the preformed crystalline LFP particles, as well as to its precursor. The PVDF polymer was dissolved in N-methylpyrrolidone prior to addition. The source of a carbon coating, final annealing temperature of the material and the synthesis method are given in the end of a sample name, for example, LFP/C-sucr-600-{I}, LFP/C-sucr-800-{I}, LFP/C-sucr-600-{II}, LFP/C-sucr-800-{II}. Chemical structures of the organic compounds used in this study as carbon sources and their denotements are given in Table 1.

Thermogravimetric analysis (TGA) was carried out using Netzsch-TG 209 F1 thermobalance in platinum crucibles in Air or Ar atmosphere. The heating rate was 10°/min. The composition of the evolved gas was identified using Netzsch Aeolos QMS 403 C mass-spectrometer. Weights of carbon residues

**Table 1.** Chemical structures and short denotements of the organic compounds used as carbon sources, and weight of carbon residues related to the weight of the organic carbon sources (wt.%) compound after pyrolysis at 600 °C.

| Organic compound | Chemical structure | Denotement | Carbon yield,% |
|---|---|---|---|
| Sucrose | 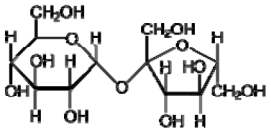 | sucr | 21.7 |
| Citric acid | 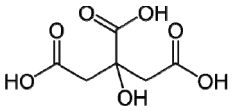 | CA | 4.8 |
| Phthalic acid | 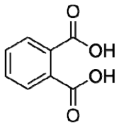 | phth | <0.1 |
| Polyvinyl alcohol | 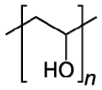 | PVA | 7.2 |
| Polyvinylpyrrolidone | 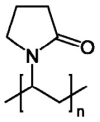 | PVP | 6.7 |
| Polyvinylidene fluoride (solution in N-methylpyrrolidone) | 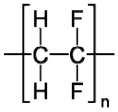 | PVDF | 36 |
| Polyethylene glycol | 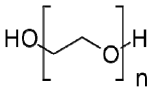 | PEG | 1.1 |
| Polyacrylic acid | 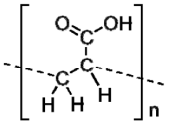 | PAA | 13.4 |

after pyrolysis of different carbon sources at 600 °C were determined using TGA (Table 1). Based on this data, the weight of carbon precursor required for the preparation of a composite containing approximately 5 wt. % carbon was calculated.

Phase composition of the samples was characterized using Rigaku D/MAX 2200 diffractometer, 40 kV/30 mA $CuK_\alpha$ radiation. Processing and qualitative analysis of the spectra was performed using Rigaku Application Data Processing and FullProf Suit software. The size of coherent scattering regions (CSR) for the reflexes with Miller indices *(311)* was calculated from peak broadening in the diffraction patterns using Scherrer equation:

$$d = \frac{k\lambda}{\sqrt{B^2 - b^2}\cos\theta}, \quad (1)$$

where $d$ is the crystallite size, $\lambda$ is the wavelength, $\theta$ is the diffraction angle, $k$ = 0.9 is the Scherrer's constant, $B$ is the half-width at half-maximum of peak, $b$ is the instrumental broadening. The instrumental broadening was determined using the $LaB_6$ SRM 660a standard. The error of CSR determination did not exceed ±2 nm.

Microstructure analysis of the samples was performed using a scanning electron microscope (SEM) Carl Zeiss NVision 40, equipped with an X-ray spectral detector Oxford X-Max, at an accelerating voltage 1 kV.

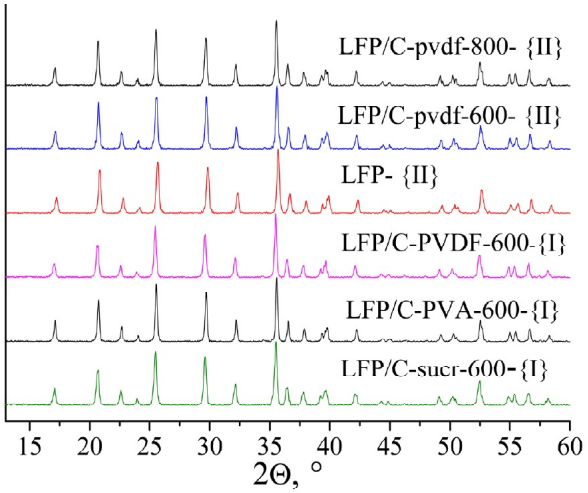


**Fig. 1.** X-ray diffraction patterns of a series of the prepared materials.

Carbon content in the composite was measured using the CHNS elemental analyzer EuroEA 3000.

The IR spectra were collected on a Nicolet iS5 IR spectrometer equipped with a Specac Quest unit; the measurements were performed in the ATR mode with the diamond ATR crystal.

Raman spectra were collected using DXRxi Raman Imaging Microscope (Thermo Fisher Scientific). A 532 nm laser was focused on the surface of the powders using a microscope lens with 50-fold magnification (beam diameter ~1 μm). Laser power was set in the range of 0.2–0.6 mW on the sample surface, in order to avoid thermal damage of the cathode materials. For every sample 50 accumulations were made, every accumulation lasting 0.5 seconds.

To prepare electrode paste, 85% LFP/C active material, 10% conductive carbon black (Timcal, Belgium) and 5% carboxymethyl cellulose (Aldrich) binder dissolved in water were thoroughly mixed. A 5 mg $cm^{-2}$ layer of the electrode was deposited on a stainless-steel net acting as a current collector. The resulting electrode was pressed under 1000 kg $cm^{-2}$ pressure and dried under vacuum at 120 °C for 8 hours.

Electrochemical testing was carried out in sealed three-electrode cells (LFP/C-Li-Li). Surface area was 2.25 $cm^2$ for the working electrode, and 5 $cm^2$ for the lithium auxiliary electrode. The cell was assembled in a glove box under the argon atmosphere with a humidity level <10 ppm. A polypropylene separator (NPO "Ufim", Moscow, Russia) was placed between the working (LFP/C) and auxiliary (Li) electrodes. A lithium reference electrode with 5.0 $cm^2$ surface area confined in an additional separator pocket, was placed between the main electrodes. A 1 M solution of $LiPF_6$ in ethylene carbonate – diethyl carbonate – dimethyl carbonate mixture with a 1:1:1 volumetric ratio served as the electrolyte. The residual water content in the electrolyte did not exceed 20 ppm (Coulometer 917, Metrohm). Electrochemical cycling of the cells was carried out at potentials ranging from from 2.5 to 4.1 V using a ZRU 50mA-10V charge/discharge system (NTC Buster, Russia). The testing was performed in a galvanostatic mode at 20-800 mA $g^{-1}$ current densities.

## 3. RESULTS AND DISCUSSION

### 3.1. Composition and morphology

X-ray diffraction patterns of the obtained LFP/C materials correspond to the orthorhombic modification of $LiFePO_4$ (*Pnma* space group, Card № 81-1173 PDF-2), which indicates that the prepared materials have olivine structure (Fig. 1). The carbon is amorphous.

When the sol-gel method is used, high-temperature annealing at ≥600 °C is required to form single-phase highly crystalline LFP. At the same time, introduction of a carbon precursor should be done before the final annealing of LFP to obtain nanomaterials. When annealing is performed in the absence of a precursor, LFP-{I} materials have CSR >100 nm and micron-sized particles are observed according to SEM data (Fig. 2a).

Introduction of a carbon precursor before the final annealing step makes it possible to obtain primary LFP particles in the nanosize range. Indeed, sucrose addition before the annealing leads to the CSR to 36 nm for LFP/C-sucr-600-{I}. The CSR size of most of the materials prepared by the sol-gel method at 600 °C is within the range from 34 to 53 nm for different carbon precursors (according to CHNS-analysis carbon content in the prepared composites is 4-9 wt.%). Therefore, along with increasing the material electrical conductivity, carbon prevents particle sintering during the annealing step. The only exceptions are LFP/C-phth and LFP/C-CA composites with the CSR sizes >100 nm and 80 nm. Carbon content in which is insufficient for preventing particle sintering (0.2 and 1.2 wt.%, respectively). Low carbon content in these composites can be explained by the volatility of the starting organic compounds or their decomposition products. For example, phthalic acid is readily dehydrated, and its anhydride boils at 295 °C

According to electron microscopy data, the size of LFP/C-600-{I} particles varies from 50 to 400 nm (Figs. 2b and 2c). These values are higher than CSR

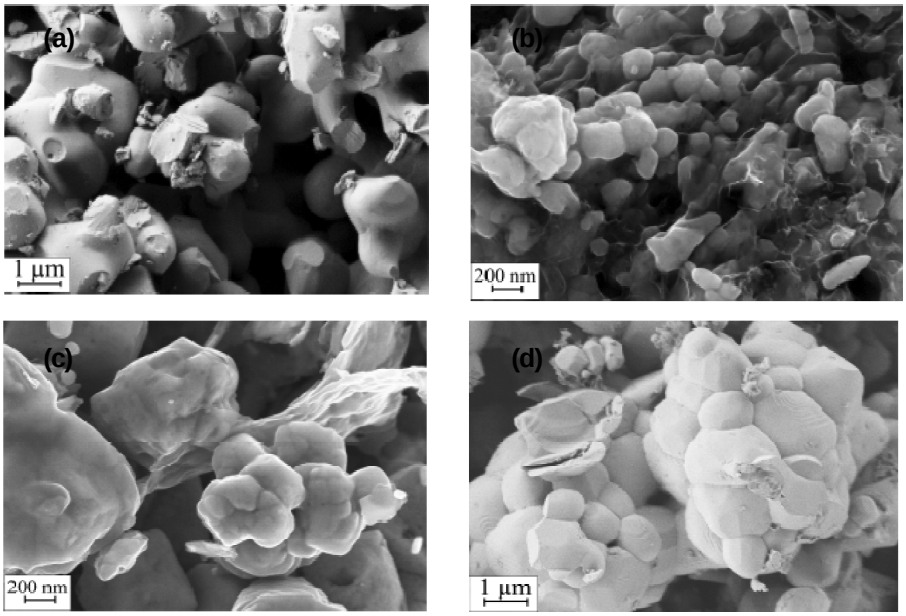


**Fig. 2.** SEM micrographs of the LFP-600-{I} (a), LFP/C-sucr-600-{I} (b), LFP/C-PAA-600-{I} (c), LFP/C-sucr-800-{I}(d) samples.

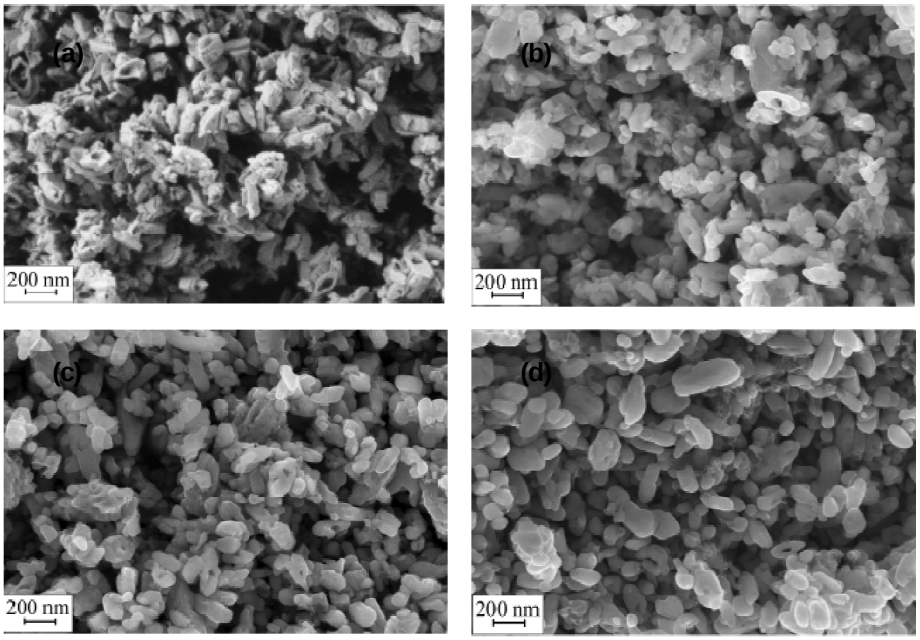


**Fig. 3.** SEM micrographs of the LFP-{II} (a), LFP/C-sucr-600-{II} (b), LFP/C-PAA-600-{II} (c), LFP/C-PAA-800-{II}(d) samples.

sizes calculated form X-ray diffraction data, from which we can conclude that the samples are agglomerates of single crystallites. Increase of the annealing temperature to 800 °C leads to the formation of LFP/C-800-{I} materials, characterized by 90-100 nm CSR size and micron-sized particles according to SEM data (Fig. 2d). In the case of annealing at 800 °C, carbon content is ~1-2 wt.% lower compared to a similar material annealed at 600 °C due to carbon burning.

When low-temperature precipitation from DMSO-water mixture is used, the resulting precipitate LFP-{II} is crystalline lithium iron phosphate with olivine structure (Fig.1) consisting of particles from ~30 to ~250 nm depending on the growth direction (Fig. 3a). In other words, using this method, nanoparticles of pure crystalline LFP without carbon coating can be prepared. In this case, the deposition of carbon coating is performed onto the pre-synthesized LFP. As follows from X-ray diffraction data, deposition of carbon coating at 600 °C does not lead to line broad-

ening in diffraction patterns. With increasing of the annealing temperature to 800 °C the pristine size of the particles increases significantly less as compared to the sol-gel method (Figs. 2d and 3d). For example, the CSR size of LFP-{II}, LFP/C-sucr-600-{II} and LFP/C-sucr-800-{II} materials was 35, 38, and 49 nm, respectively.

Completeness of the pyrolysis was monitored using TGA with evolved gas mass-spectrometry. Characteristic curves of mass loss upon LFP/C heating in air are given in Fig. 4. Upon heating of LFP/C at temperatures above 100 °C, a mass loss is observed, coupled with water elimination (*m*/*z* = 18) adsorbed on the surface. At temperatures above 250 °C, according to mass-spectrometry data, carbon dioxide elimination starts (*m*/*z* = 44). It is coupled with a mass increase (Fig. 4a). We believe this indicates that a considerable fraction of the eliminated $CO_2$ is adsorbed on the LFP surface. The maximum rate of carbon dioxide emission is observed at temperatures 390-490 °C depending on the carbon source. It is accompanied by the end of mass gain, and after 410-490 °C mass loss starts. As follows from X-ray diffraction data, upon heating of LFP above 500 °C oxidation of divalent iron occurs, leading to the formation of final thermolysis products $Fe_2O_3$ and $Li_3Fe_2(PO_4)_3$ [60,61].

In addition, the gaseous products of annealing in air for all LFP/C samples synthesized at 600 °C, apart from $CO_2$, reveal water elimination at 250-570 °C. For the samples synthesized at 800 °C, water elimination in this temperature interval is ~3 times less vigorous. The obtained data indicate that pyrolysis processes at 600-800 °C are incomplete. An attempt to carry out the synthesis at 900 °C resulted in melting of the samples.

It can be concluded that with the increase of the final annealing temperature to 800 °C the pyrolysis proceeds to a greater degree. This assumption is verified by IR-spectroscopy data. For example, the IR-spectra of sucrose pyrolysis product at 600 °C contains residual bands at 1000 $cm^{-1}$ and 3500 $cm^{-1}$ corresponding to stretching vibrations of C-O and O-H groups, respectively. As a result of annealing at 800 °C, peaks of the initial compounds disappear almost completely.

We demonstrated previously that the surface of LFP is partially fluorinated when PVDF is used as a source for carbon coating [19]. At the same time, upon heating of such materials in air above 530 °C a mass loss is observed, coupled with fluorine emission (*m*/*z*=19). A similar effect was observed for deposition of a carbon coating onto lithium titanate using PVDF as a precursor [60].

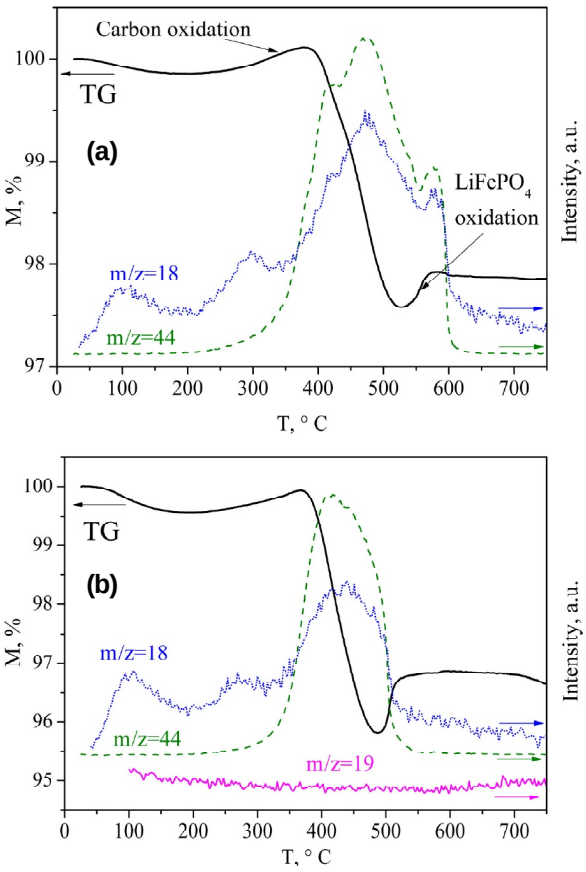


**Fig. 4.** Thermogravimetric curves (TG) and intensities of evolved gas flow versus temperature obtained for LFP/C-PVA-600-{II} (a), LFP/C-PVDF-600-{II} (b) and LFP/C-PVDF-800-{II} (c). The numbers adjacent to curves indicate mass numbers (m/z) for respective ions.

On heating LFP/C-PVDF-600-{II} (Fig. 4b) and LFP/C-PVDF-800-{II} samples in air no significant fluorine emission is observed. It indicates that for deposition of PVDF solution onto crystalline LFP fluorination of phosphate surface scarcely occurs.

In the obtained Raman spectra an intensive band with a maximum at ~1590 $cm^{-1}$ can be assigned to the G-band of crystalline graphite ($sp^2$-hybridized carbon) and a band at ~1350 $cm^{-1}$ to the D-band of disordered graphite (Figs. 5a-5c) [61]. Integral intensity of these lines is denoted as I($sp^2$). Along with them, two wide bands can be distinguished around 1200 and 1500 $cm^{-1}$ (Fig. 5d), corresponding to the carbon fragments with different structure (I(dif)). For example, the band at 1500 $cm^{-1}$ is associated with vibrations of $sp^3$-hybridized carbon [61,62]. For the materials obtained at 600 °C the ratio I($sp^2$)/I(dif) varies from 1.11 to 1.56, indicating that carbon coating is mostly represented by the graphite structure, which has high electron conductivity [56,64-66]. The LFP/C-PVP-600-{I} material is

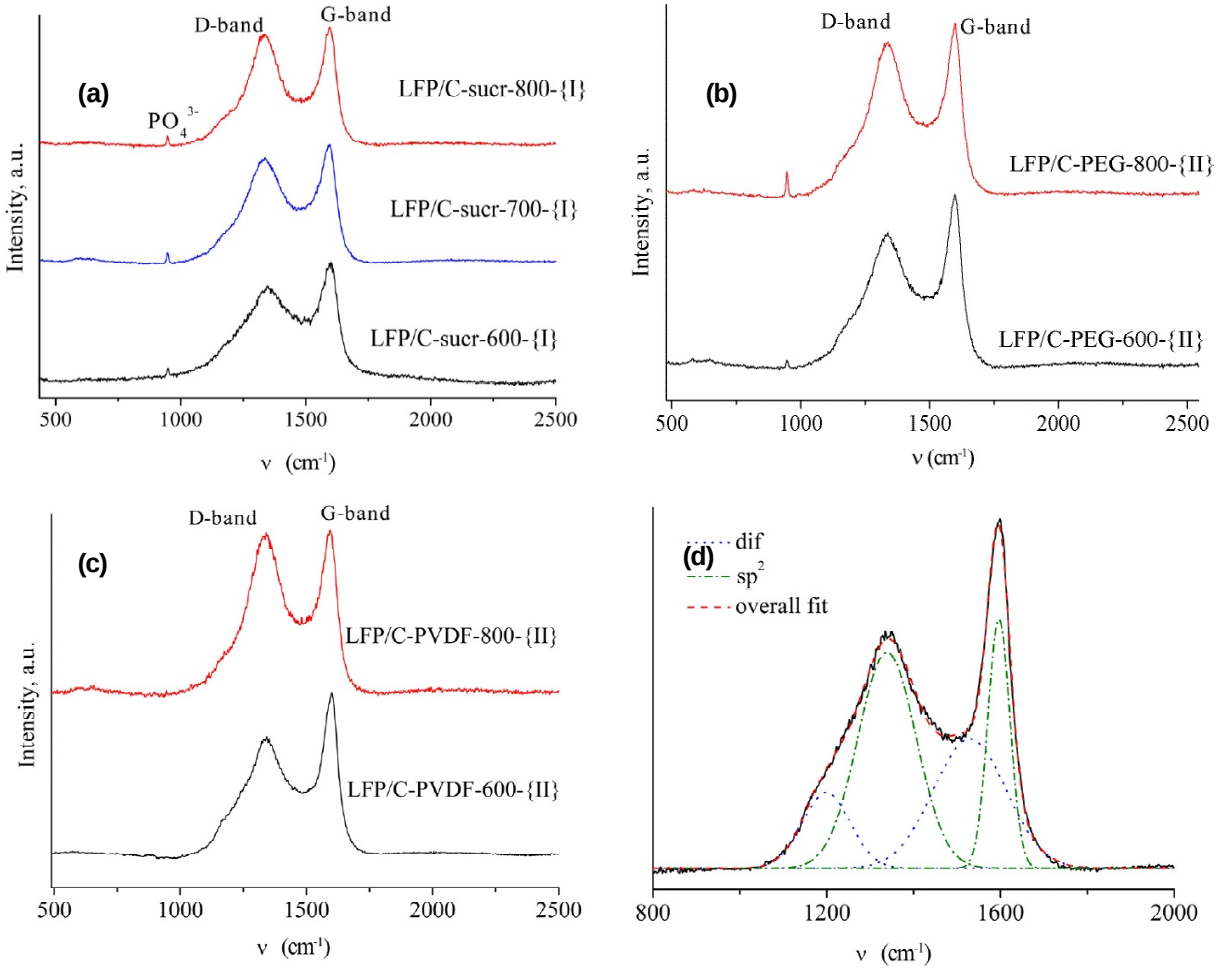


**Fig. 5.** Raman spectra of LFP/C samples with a carbon coating obtained at 600 and 800 ºC using various carbon sources: sucr (a), PEG (b), PVDF (c). For the LFP/C-PVA-600-{II} sample, a spectral curve fitting is demonstrated (d).

an exception, having $I(sp^2)/I(dif)=0.98$. With increasing the annealing temperature from 600 to 800 °C, the intensity of additional bands in Raman spectra decreases. This indicates a certain perfection of graphite structure is observed. In this case $I(sp^2)/I(dif)$ ratio increases ($1.23 \leq I(sp^2)/I(dif) \leq 1.75$) as well as the depth of the "dip" between the D- and G-bands (Fig.5) [64].

It is worth noting that although the carbon content is relatively similar in the investigated LFP/C-800 samples, intensities of the bands at 950 $cm^{-1}$, corresponding to vibrations of $PO_4^{3-}$ groups, are significantly lower in the case of carbon coating obtained from PVDF. This can indicate that when PVDF is used, the carbon coating is more uniform and thus hinders the penetration of a beam to the LFP surface.

Therefore, we can conclude that as the treatment temperature increases, an improvement of carbon coating occurs. However, the growth of the pristine particles of the material is observed along with this. Moreover, the agglomeration degree of the pristine particles increases (to micron size according to SEM data). This effect is more pronounced for the materials prepared by the sol-gel method. The agglomeration degree of the pristine particles in the sol-gel synthesis also depends on the carbon source. It was the most pronounced when polyacrylic acid or polyethylene glycol were used, and the least pronounced when sucrose or polyvinylidene fluoride were used.

## 3.2. Electrochemical testing

Characteristic charge and discharge curves of the obtained materials are shown in Fig. 6 by the example of LFP/C-{II}. Their shape is almost identical and is characteristic of $LiFePO_4$-based cathode materials. The charge/discharge curves feature a plateau that corresponds to the $Fe^{2+} \leftrightarrow Fe^{3+}$ transition at the potential of ~3.4 V. As follows from the obtained data, no correlation is observed between

the CSR size *(d)* in the interval 30 < *d* < 60 nm and the capacity measured at a low current of 20 mA $g^{-1}$. For the CSR > 80 nm a sharp decrease of capacity is observed. At low charge/discharge rate, the discharge capacity values vary from 96 to 161 mAh $g^{-1}$ and are primarily determined by the degree of agglomeration of pristine particles. Lower capacity values were obtained for the LFP/C-PAA-600-{I} material, which was characterized by the largest agglomerate sizes according to SEM data. For the materials LFP/C-sucr-600-{II}, LFP/C-PEG-600-{II}, LFP/C-PVA-600-{II}, LFP/C-PVDF-600-{I}, LFP/C-PVDF-600-{II}, LFP/C-PVDF-800-{II}, the obtained discharge capacities range from 157 to 161 mAh $g^{-1}$. Taking into consideration the carbon (which is electrochemically inactive in the potential window 2.5 – 4.1 V) content in the composites, the obtained capacities are close to the theoretical value.

When the current density is increased, the discharge capacity of LFP/C is reduced. Cycling data at different current densities for some of the LFP/C samples are shown in Fig. 7. Lowering $LiFePO_4$ capacity with increasing current density is associated with kinetic factors rather than material degradation. Since the capacity is restored almost to its initial value after cycling at high currents and back to low current.

In the case of the sol-gel synthesis {I}, the highest capacities for both low and high charge/discharge rates are obtained for the material synthesized at 600 °C using PVDF (Fig. 7 (1)). Better performance of this material compared to the other ones is associated with higher homogeneity of carbon coating obtained by PVDF pyrolysis, and higher electrical conductivity of the material due to partial fluorination of the phosphate [19]. Discharge capacity of LFP/C- PVDF-600-{II} is 160, 104 and 70 mA $g^{-1}$ at current densities of 20, 200 and 800 mAh $g^{-1}$.

In the case of low-temperature precipitation from DMSO {II}, superior discharge capacity values are obtained using PEG as the carbon source (Fig. 7 (2)) due to a higher content of carbon in the form of graphite and consequently better electrical conductivity (I($sp^2$)/I(dif)=1.56). Discharge capacity of LFP/C-PEG-600-{II} is 158, 131 and 77 mAh $g^{-1}$ at current densities of 20, 200, and 800 mA $g^{-1}$.

For both the sol-gel synthesis {I} and low-temperature precipitation from DMSO {II}, higher capacities at increased charge/discharge rates were obtained for the materials synthesized at 600 °C, which is associated with smaller particle sizes of these materials (Fig. 7 (2,3)).

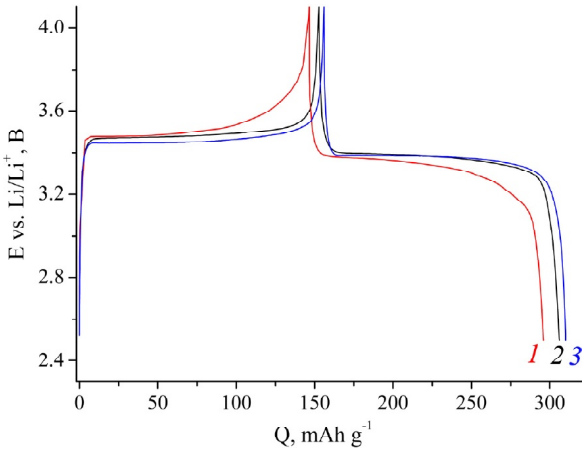


**Fig. 6.** Charge/discharge curves of LFP/C-600-{II} obtained using PVP *(1)*, sucr *(2)* and PEG *(3)* as the carbon source. Current density is 20 mA $g^{-1}$.

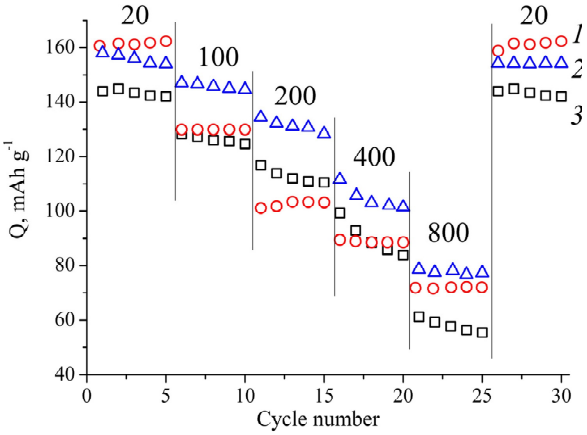


**Fig. 7.** Change of discharge capacity during cycling of LFP/C-PVDF-600-{I} *(1)* LFP/C-PEG-600-{II} *(2)* and LFP/C-PEG-800-{II} *(3)* samples. Current densities (mA $g^{-1}$) are given in the figure (I(*charge*)=I(discharge)).

## 4. CONCLUSION

In summary, formation of composite materials with carbon results in enhanced electrical conductivity at the grain boundary. Moreover, the preparation of more finely dispersed materials is observed in the case of addition of a carbon source before the high-temperature annealing. This shortens the diffusion path length for the charge carriers and promotes more efficient deintercalation/intercalation of lithium cations during charge/discharge. Carbon coating efficiency is determined by its electrical conductivity, as well as the ability of the additive to prevent particle sintering during the annealing. In order to obtain more efficient cathode material capable of faster charge/discharge, it is necessary to increase

charge transfer in the bulk of LFP particles also. This can be achieved by combining the surface (carbon coating) and bulk (doping) modifications.

## ACKNOWLEDGEMENT

The present work was financially supported by Russian foundation for basic research (project 16-29-05241). This work was performed using the equipment of the Joint Research Centre of IGIC RAS.

## REFERENCES

[1] A.K. Padhi, K.S. Nanjundaswamy and J.B. Goodenough // J. *Electrochem. Soc.* **144** (1997) 1188.
[2] R. Amin, J. Maier, P. Balaya, D. Chen and C. Lin // *Solid State Ionics* **179** (2008) 1683.
[3] S. Zhang, J. Zhang, S. Xu, X.Yuan and B. He // *Electrochim. Acta* **88** (2013) 287.
[4] D.V. Safronov, S.A. Novikova, A.B. Yaroslavtsev and A.M. Skundin // *Inorg. Mater.* **48** (2012) P. 57.
[5] A. Eftekhari // *J. Power Sources* **343** (2017) 395.
[6] D.V. Safronov, I.Y Pinus, I.A. Profatilova, V.A. Tarnopol'skii, A.M. Skundin and A.B. Yaroslavtsev // *Inorg. Mater.* **47** (2011) 303.
[7] K. Zaghib, A. Guerfi, P. Hovington, A. Vijh, M. Trudeau, A. Mauger, J.B. Goodenough and C.M. Julien // *J. Power Sources* **232** (2013) 357.
[8] A.B. Yaroslavtsev, T.L. Kulova and A.M. Skundin // *Russ. Chem. Rev*. **84** (2015) 826.
[9] S.A. Novikova and A.B. Yaroslavtsev // *Rev. Adv. Mater. Sci.* **49** (2017) 129.
[10] A. Örnek, E. Bulut, M. Can and M. Özacar // *J. Solid State Electrochem.* **17** (2013) 3101.
[11] S. Novikova, S. Yaroslavtsev, V. Rusakov, T. Kulova, A. Skundin and A. Yaroslavtsev // *Electrochim. Acta* **122** (2014) 180.
[12] W. Liu, Q. Huang and G. Hu // *J. Alloys Compd.* **632** (2015) 185.
[13] S. Novikova, S. Yaroslavtsev, V. Rusakov, A. Chekannikov, T. Kulova, A. Skundin and A. Yaroslavtsev // *J. Power Sources* **300** (2015) 444.
[14] Q. Liu, W. Liu, D. Li and Z. Wang // *Mater. Lett.* **162** (2016) 87.
[15] O. A. Drozhzhin, V. D. Sumanov, O. M. Karakulina, A. M. Abakumov, J. Hadermann, A. N. Baranov, K. J. Stevenson and E. V. Antipov // *Electrochim. Acta* **191 (**2016) 149.
[16] L. Li, L. Wu, F. Wu, Sh. Song, X. Zhang, Ch. Fu, D. Yuan and Y. Xiang ***//*** *J. Electrochem. Soc.* **164** (2017) A2138.
[17] Z.-Y. Chen, H.-L. Zhu, S. Ji, R. Fakir and V. Linkov // *Solid State Ionics* **179** (2008) 1810.
[18] H. Li and H. Zhou // *Chem. Commun*. **48** (2012) 1201.
[19] D. Gryzlov, S. Novikova, T. Kulova, A. Skundin and A. Yaroslavtsev // *Mater. Design* **104** (2016) 95.
[20] X. Tu, Y. Zhou and Y. Song // *Appl Surf Sci*. **400** (2017) 329.
[21] Z. Caban-Huertas, D.P. Dubal, O. Ayyad and P. Gomez-Romero // *J Electrochem. Soc.*, **164** (2017) A6140.
[22] Y.-H. Huang and J.B. Goodenough // *Chem. Mater.* **20** (2008) 7237.
[23] A. Fedorková, R. Oriňáková, Andrej Oriňák, I. Talian, Andreas Heile, H.-D. Wiemhöfer, D. Kaniansky and H. F. Arlinghaus // *J. Power Sources* **195** (2010) 3907.
[24] N. Vicente, M. Haro, D. Cíntora-Juárez, C. Pérez-Vicente, J. L. Tirado, Sh. Ahmad and G. Garcia-Belmonte // *Electrochim. Acta* **163** (2015) 323.
[25] H. Li and H. Zhou // *Chem. Commun*. **48** (2012) 1201.
[26] G. Kucinskis, G. Bajars and J. Kleperis // *J. Power Sources* **240** (2013) 66.
[27] K. Wu, G. Hun, K. Dun, Zh. Peng and Y. Cao // *Ceram. Int.* **41 (**2015) 13867.
[28] G. Wang, Zh. Ma, G. Shao, L. Kong and W. Gao // *J. Power Sources* **291** (2015) 209.
[29] K. Christmann, *Introduction to Surface Physical Chemistry* (Springer, Darmstadt: Steinkopff, New York, 1991).
[30] F. A. Kröger, *The Chemistry of Imperfect Crystals* (North-Holland Publishing Company, 1974),.
[31] H. Gao, L. Jiao, J. Yanga, Z. Qi, Y. Wang and H. Yuan // *Electrochim. Acta* **97** (2013) 143.
[32] Y. Ge, X. Yan, J. Liu, X. Zhang, J. Wang, X. He, R. Wang and H. Xie // *Electrochim. Acta* **55** (2010) 5886.
[33] A. Örnek and O. Efe // *Electrochim. Acta* **166** (2015) 338.
[34] K.-X. Wang, X.-H. Li and J.-Sh. Chen // *Adv. Mater.* **27** (2015) 527.
[35] Y.-H. Huang and J.B. Goodenough // *Chem. Mater.* **20** (2008) 7237.

[36] D. Cíntora-Juárez, C. Pérez-Vicente, S. Ahmad and J.L. Tirado // *RSC Advances* **4** (2014) 26108.
[37] N. Vicente, M. Haro, D. Cíntora-Juárez, C. Pérez-Vicente, J. Luis Tirado, Sh. Ahmad and G. Garcia-Belmonte // *Electrochim. Acta* **163 (**2015) 323.
[38] D. Lepage, Ch. Michot, G. Liang, M. Gauthier and S. B. Schougaard // *Angew. Chem*. **123** (2011) 7016.
[39] H. Li and H. Zhou // *Chem. Commun.* **48** (2012) 1201.
[40] X. Lei, H. Zhang, Y. Chen, W. Wang, Y. Ye, C. Zheng, P. Deng and Z. Shi // *J Alloy Compd*. **626** (2015) 280.
[41] Y. Su, Y. Liu, P. Liu, D. Wu, X. Zhuang, F. Zhang and X. Feng // *Angew. Chem. (Int. Ed.)* **54 (**2015) 1812.
[42] G. Qin, Q. Ma and C. Wang // *Solid State Ionics* **257** (2014) 60.
[43] T. Liu, F. Cao, L. Ren, X. Li, S. Sun, X. Sun, Z. Zang, Q. Niu and J. Wu // *J. Electroanal. Chem.* **807** (2017) 52.
[44] G. Liang, L. Wang, X. Ou, X. Zhao and S. Xu // J. Power Sources. **184 (**2008) 538.
[45] J. Wang, Zh. Shao and H. Ru // *Ceram. Int*. **40** (2014) 6979.
[46] G.T.-K. Fey and T.-L. Lu // *J. Power Sources* **178 (**2008) 807.
[47] M. Kuzmanović, D. Jugovića, M. Mitrić, B. Jokić, N. Cvjetićanin and D. Uskoković // *Ceram. Int.* **41** (2015) 6753.
[48] A. Örnek, E. Bulut and M. Özacar // *Ceram. Int.* **40** (2014) 15727.
[49] W. Jianmei, C. Feipeng, Y. Gai, W. Bo, H. Suqin // *Mater. Eng.* **44** (2015) 307.
[50] J. Du, L.-B. Kong, H. Liu, J.-B. Liu, M.-Ch. Liu, P. Zhang, Y.-Ch. Luo and L. Kang // *Electrochim. Acta* **123** (2014) 1.
[51] E. Avci, M. Mazman, D. Uzun, E. Bicer and T. Sener // *J. Power Sources* **240** (2013) 328.
[52] S. El Khakani, D. Rochefort and D. D. MacNeil // *J. Electrochem. Soc*. **163** (2016) A1311.
[53] M. M. Doeff, J. D. Wilcox, R. Yu, A. Aumentado, M. Marcinek and R. Kostecki // *J. Solid State Electrochem.* **12 (**2008) 995.
[54] Y.-H. Nien, J.R. Carey and J.-S. Chen // *J. Power Sources* **193 (**2009) 822.
[55] P. Swain, M. Viji, P. S. V. Mocherla and C. Sudakar // *J. Power Sources* **293 (**2015) 613.
[56] Y.-H. Nien, J.R. Carey and J.-S. Chen // *J. Power Sources* **193** (2009) 822.
[57] M. L. Kaplan, P. H. Schmidt, Ch.-H. Chen and W. M. Walsh, Jr. // *Appl. Phys. Lett.* **36** (1980) 867.
[58] C. Delacourt, P. Poizot and C. Masquelier, *Crystalline nanometric $LiFePO_4$* (US Patent, Published Oct. 2nd 2008, 20080241690 A1).
[59] A. Svitan'ko, V. Scopets, S. Novikova and A. Yaroslavtsev // *Solid State Ionics* **271** (2015) 42.
[60] I. A. Stenina, A. N. Sobolev, A. A. Kuz'mina, T. L. Kulova, A. M. Skundin, N. Yu. Tabachkova and A. B. Yaroslavtsev // *Inorg. Mater.* **53** (2017) 1039.
[61] J.D. Wilcox, M.M. Doeff, M. Marcinek and R. Kostecki // *J. Electrochem. Soc.* **154** (2007) A389.
[62] R.P. Vidano and D.B. Fishbach // *Solid State Comm.* **39** (1981) 341.
[63] I.A. Stenina, S.S. Bukalov, T.L. Kulova, A.M. Skundin, N.Y. Tabachkova and A.B. Yaroslavtsev // *Nanotechnologies in Russia* **10** (2015) 865.
[64] M. M. Doeff, Y. Hu, F. McLarnon and R. Kostecki // *Electrochemical and Solid-State Letters* **6** (2003) A207.
[65] Sh. Tao, P. Cui, W. Huang, Zh. Yu, X. Wang, D. Liu, L. Song, W. Chu and Sh. Wei // *Carbon* **96** (2016) 1028.
[66] J. Song, B. Sun, H. Liu, Zh. Ma, Zh. Chen, G. Shao and G. Wang // *ACS Appl. Mater. Interfaces* **8** (2016) 15225.